Supporting information

Solution-Processed High-k Photopatternable Polymers for Low-voltage Electronics

*Qingqing Sun, Hongwei Ge, Shuai Wang, Xiaohang Zhang, Juzhong Zhang, Shisheng Li, Zhiqiang Yao, Lei Zhang, Xuying Liu**

Q. Sun, H. Ge, S. Wang, X. Zhang, J. Zhang, Z. Yao, X. Liu

School of Materials Science and Engineering, State Key Laboratory of Structural Analysis, Optimization and CAE Software for Industrial Equipment, National Engineering Research Center for Advanced Polymer Processing Technology

Zhengzhou University, Zhengzhou 450001, China

Email: liuxy@zzu.edu.cn

S. Li,

Research Center for Functional Materials, National Institute for Materials Science (NIMS), Tsukuba, Ibaraki 305-0044, Japan.

L. Zhang,

Beijing Advanced Innovation Center for Soft Matter Science and Engineering,

Beijing University of Chemical Technology, Beijing 100029, China.

Table S1. Molecular weight and distribution of P(CEA-co-HDDA) prepolymers

CEA:HDDA	Mn	Mw	PDI
9:1	11834	26386	2.14
8:2	16013	58397	3.64
7:3	20108	100082	4.97
6:4	24393	106823	4.37

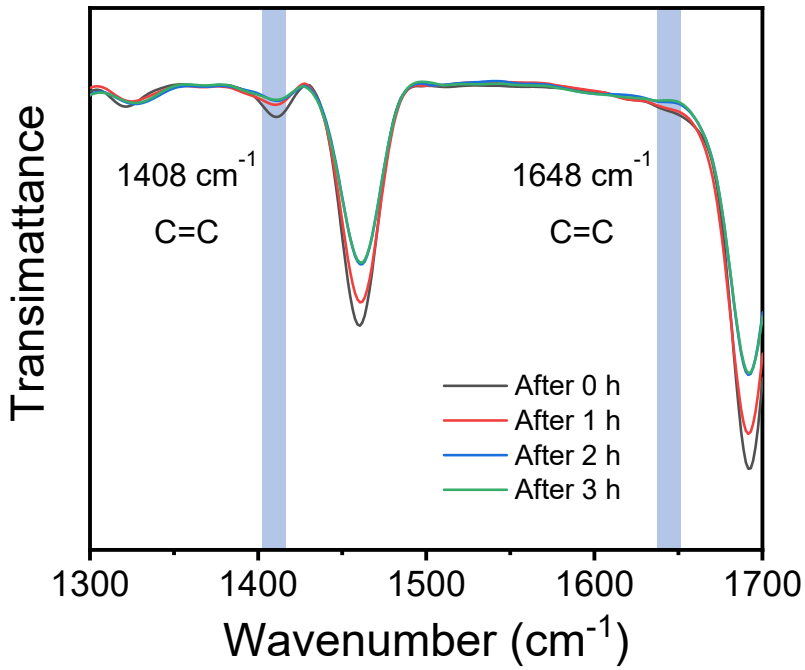

Fig. S1 The FTIR characterization of P(CEA-co-HDDA) polymers with different UV time treatment. The blue region shows that C=C bonds are gradually cross-linked, thus synthesizing target polymers.

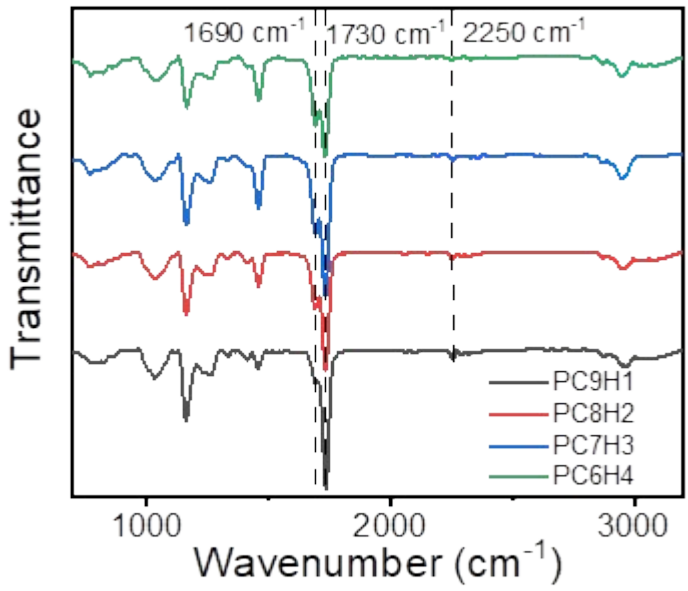

Fig. S2. The FTIR spectrum of P(CEA-co-HDDA) polymers with different mass ratios. The peaks at the wavelength of 2250 cm^{-1} are assigned to the stretching mode of -CN groups.

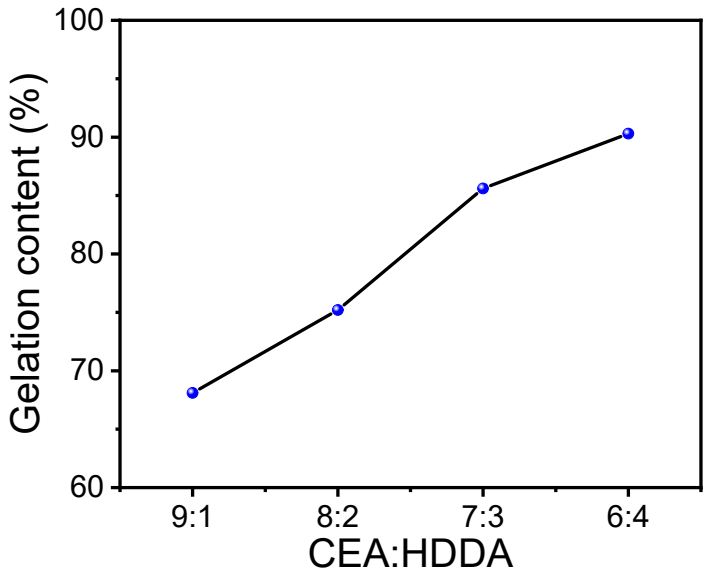

Fig. S3 The gel content characterization of P(CEA-co-HDDA) polymers with different mass ratios. It is clear that the gelation content strongly depends on the mass ratio of CEA and HDDA. Higher loading of HDDA yields higher gelation content.

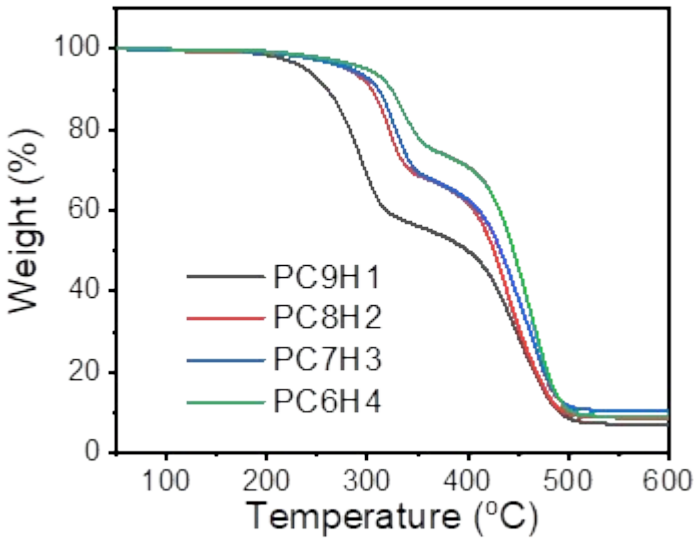

Fig. S4 TGA curves of P(CEA-co-HDDA) polymer with different mass ratios. As observed, when increasing the cross-linking degree, the decomposition temperature was increased to be as high as 300°C.

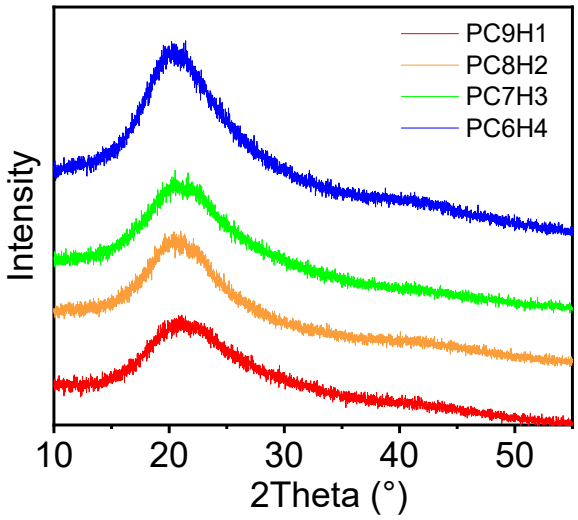

Fig. S5 The crystallization characterization of the P(CEA-co-HDDA) polymers by X-ray Diffraction (XRD).

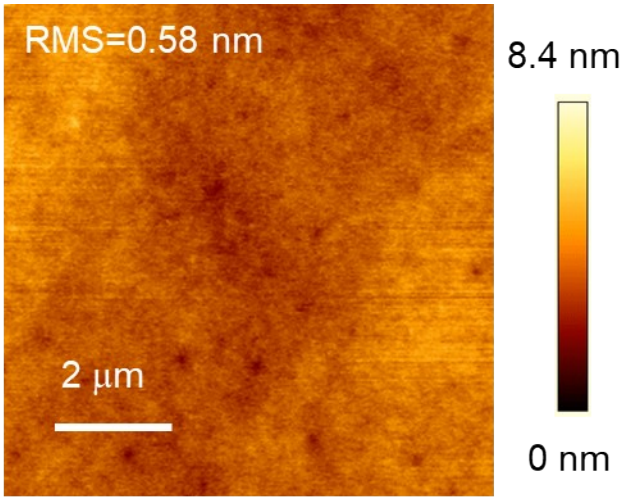

Fig. S6 The Atomic Force Microscope (AFM) scanning on the dielectric film PC6H4 surface.

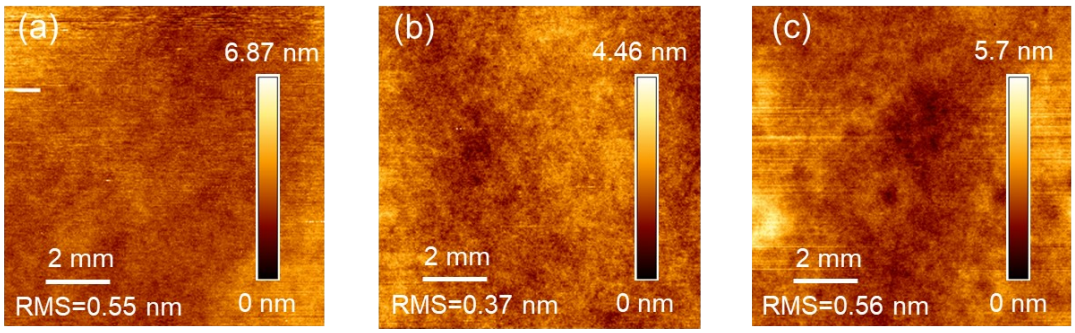

Fig. S7 The surface morphology characterization by AFM of P(CEA-co-HDDA) polymers with the mass ratio of CEA and HDDA: (a) 9-1, (b) 8-2, (c) 7-3. These results suggest that the deposited polymer films are well uniform, pinhole-free, and exhibit very smooth surface.

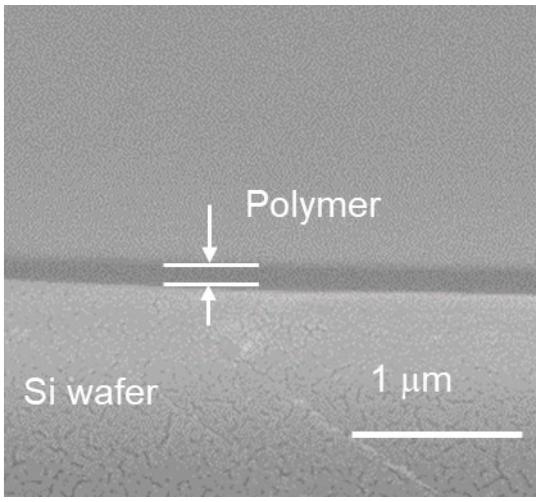

Fig. S8 The Scanning Electron Microscope (SEM) characterization on the cross-section of the P(CEA-co-HDDA) polymer on a silicon wafer.

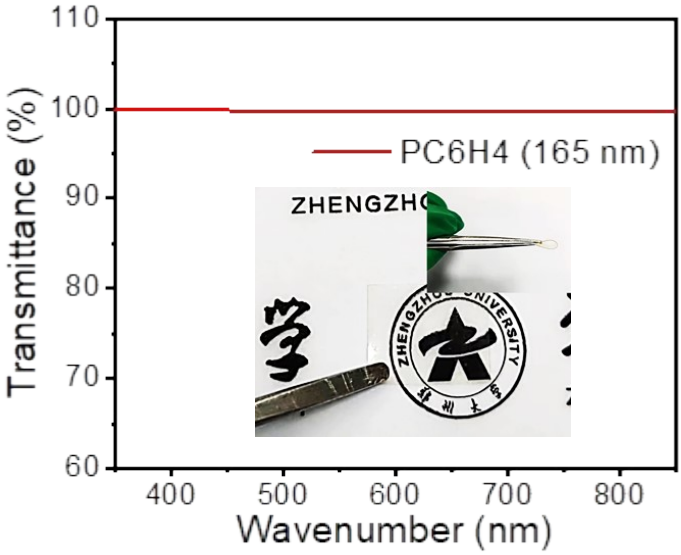

Fig. S9 The optical transmittance measurement of the PC6H4 film with the inserted optical photograph on the flexible polyethylene naphthalate substrate.

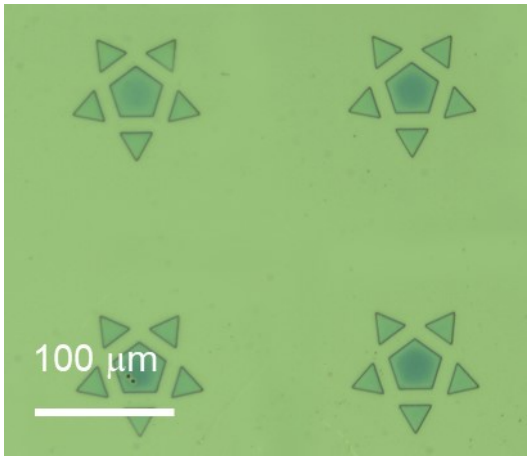

Fig. S10 he optical photograph of the patterned dielectric film with complex structures and features.

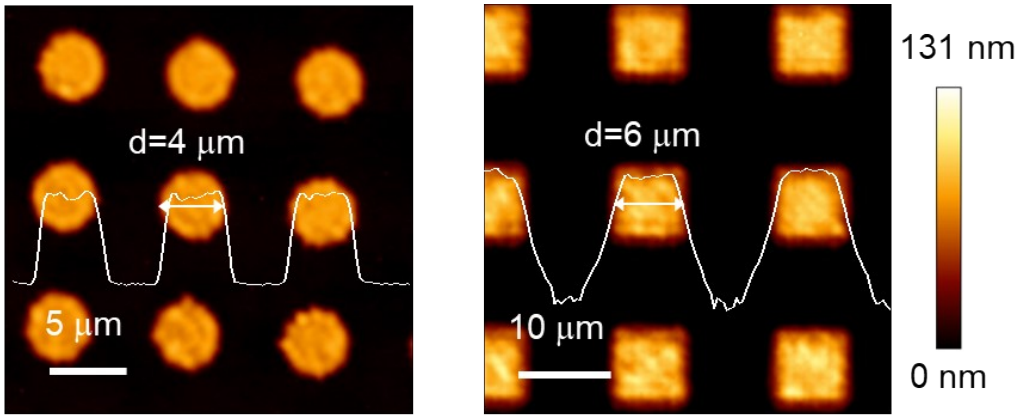

Fig. S11 The surface morphology characterization of high-resolution patterned polymers by AFM with the responsive profile curves inserted

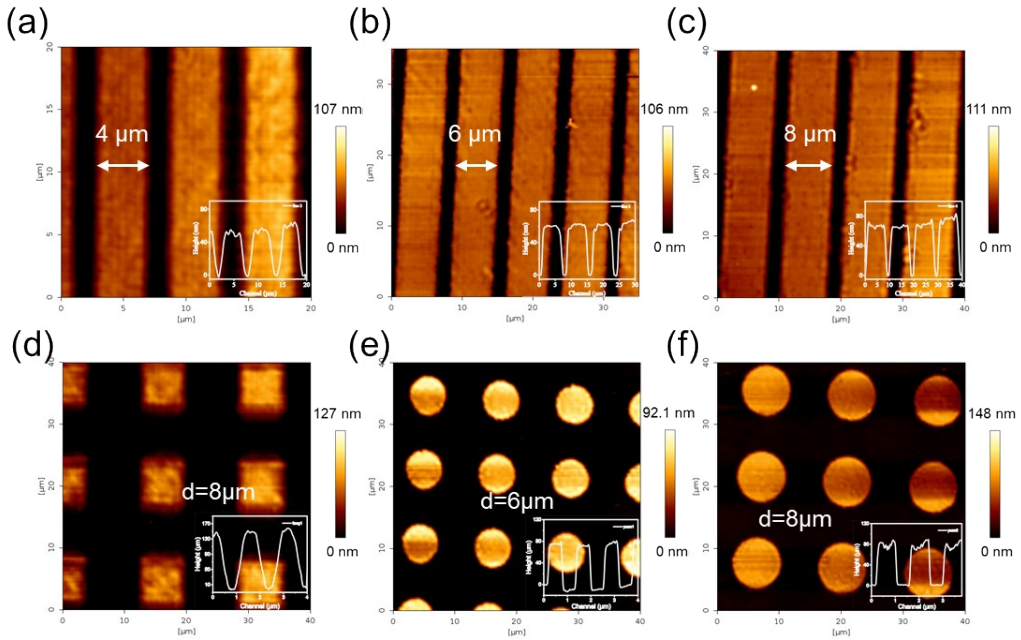

Fig. S12 The surface morphology characterization of high-resolution patterned polymers by AFM with the responsive profile curves inserted: (a-c) strip-shaped patterns of different widths; (d-f) square/circle-shaped patterns of different diameters. These patterns can be clearly characterized, showing very sharp edge and flat surface.

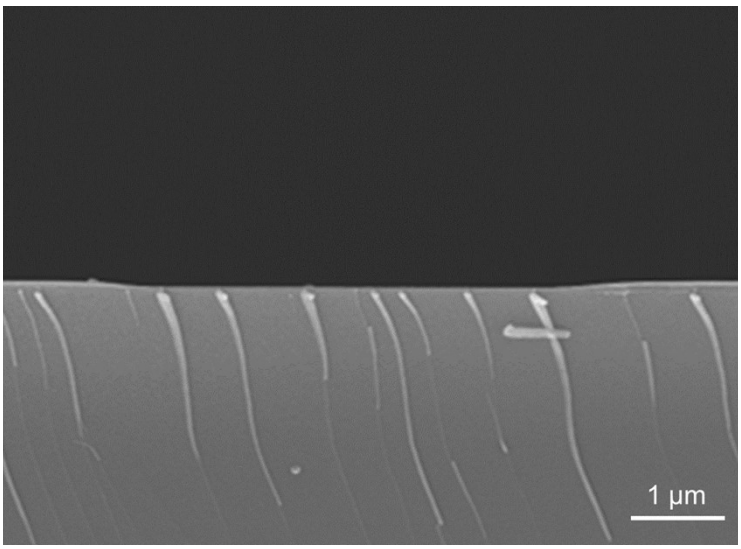

Fig. S13 The cross-section characterization of the patterned polymer dielectric by SEM. It can be observed that the polymer film shows dense structure, uniform thickness, and free-defect features.

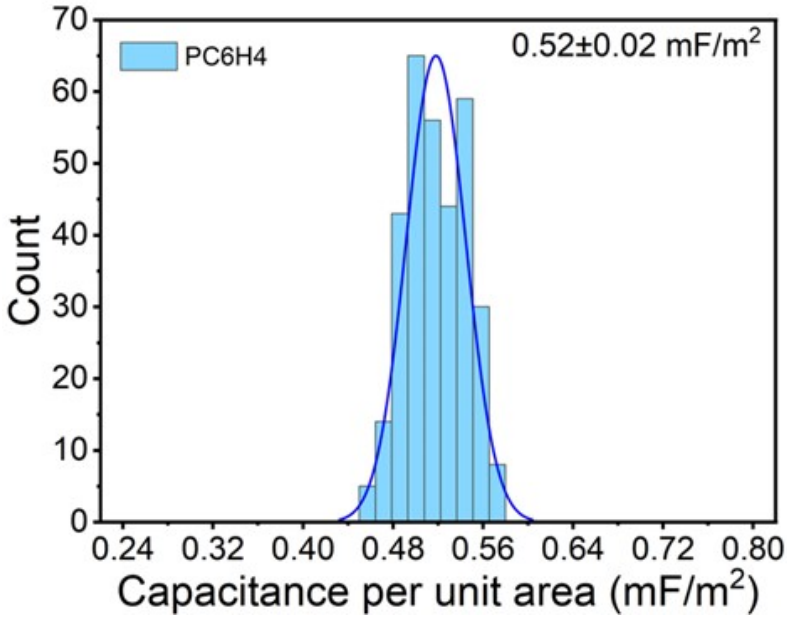

Fig. S14 Histogram showing the distribution of capacitance obtained from 324 devices on a wafer scale.

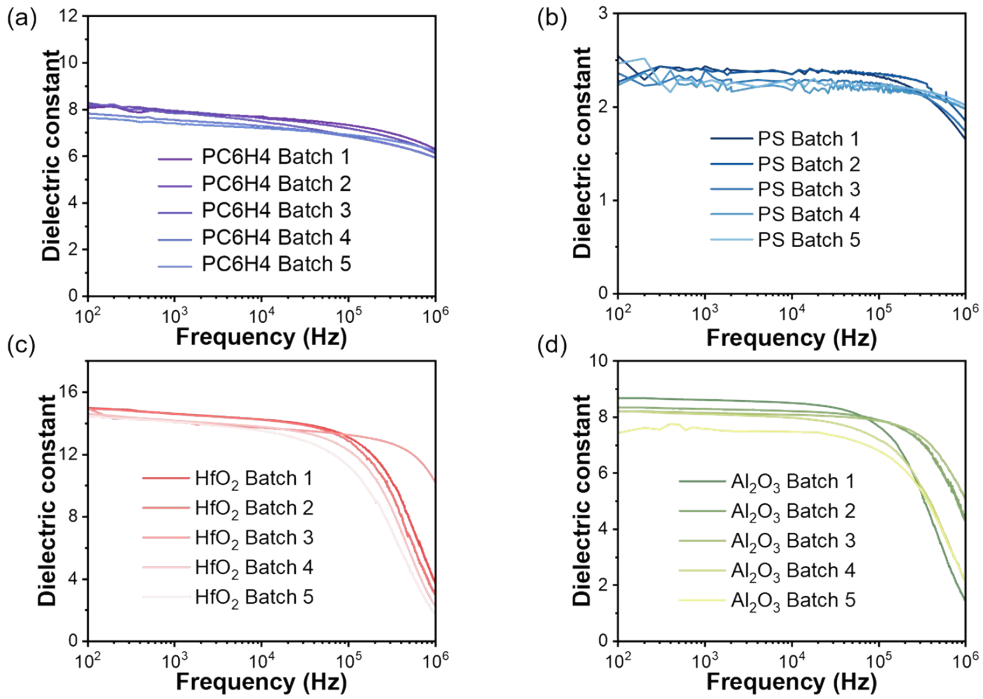

Fig. S15 Dielectric constants for different batches of (a) PC6H4, (b) Polystyrene (PS), (c) hafnium oxide (HfO_2), (d) aluminium oxide (Al_2O_3).

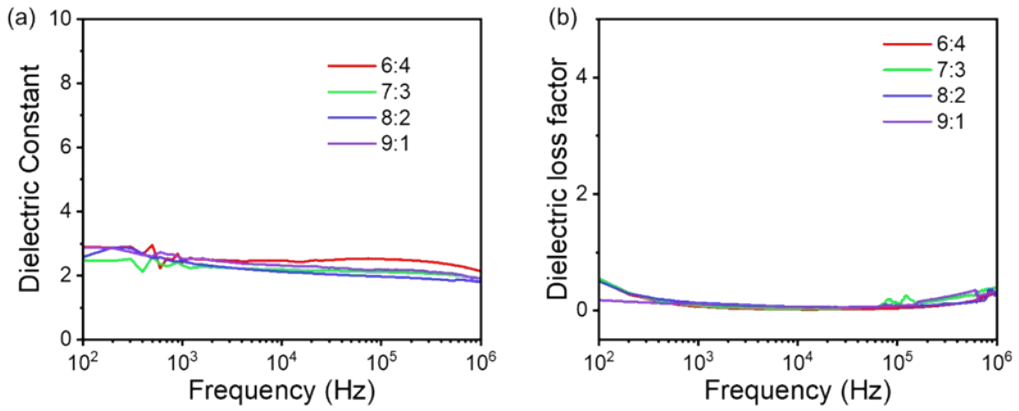

Fig. S16 Dielectric properties of polymer dielectric films made with n-propyl acrylate as monomer (a) Dielectric constant, (b) Dielectric loss factor.

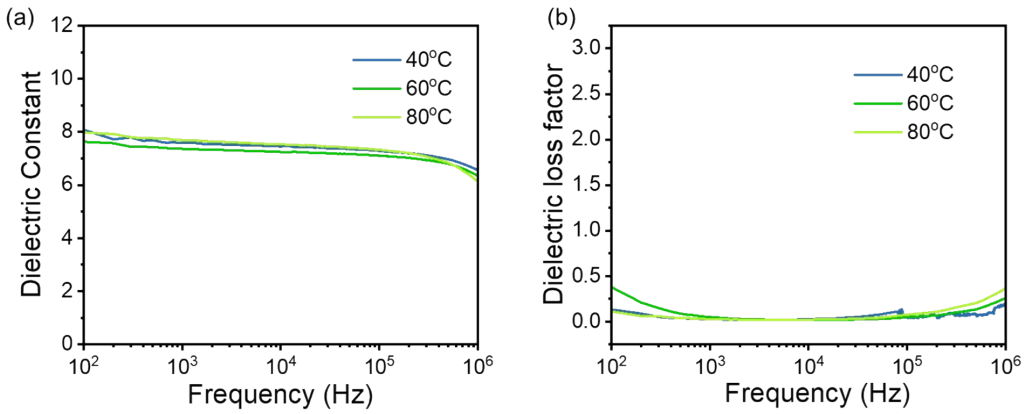

Fig. S17 Dielectric properties of UV cross-linked PC6H4 films at different temperatures (a) Dielectric constant, (b)Dielectric loss factor.

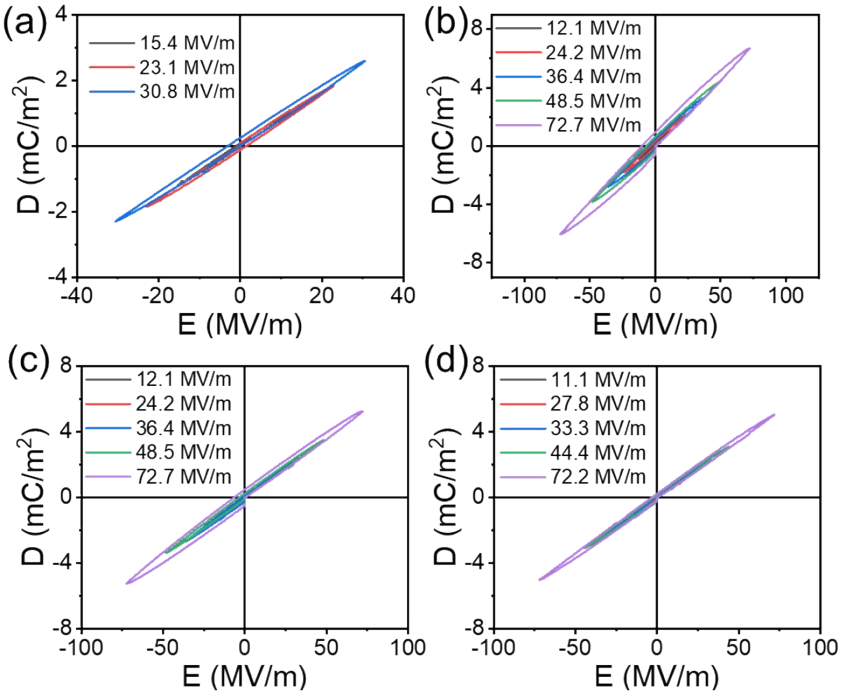

Fig. S18 Bipolar *D-E* loops of different P(CEA-co-HDDA) polymer films: (a) 9-1; (b) 8-2; (c) 7-3; (d) 6-4. When decreasing the CEA content, the *D-E* loop is clearly observed to become narrow, which can be understood that the related energy loss in charge-discharge process is suppressed.

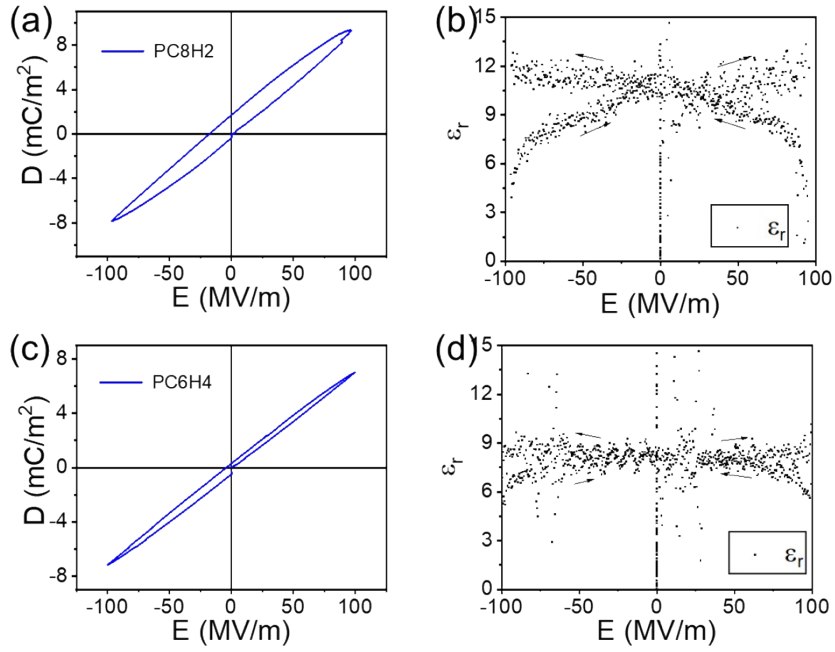

Fig. S19 Bipolar *D-E* loops and corresponding dynamic dielectric constant-electric

field curves of the P(CEA-co-HDDA) polymers with the mass ratio of (a, b) 8-2 and (c, d) 6-4. As observed, when increasing the electrical field, the PC6H4 shows narrower loop than PC8H2, suggesting a much stabler dielectric performance.

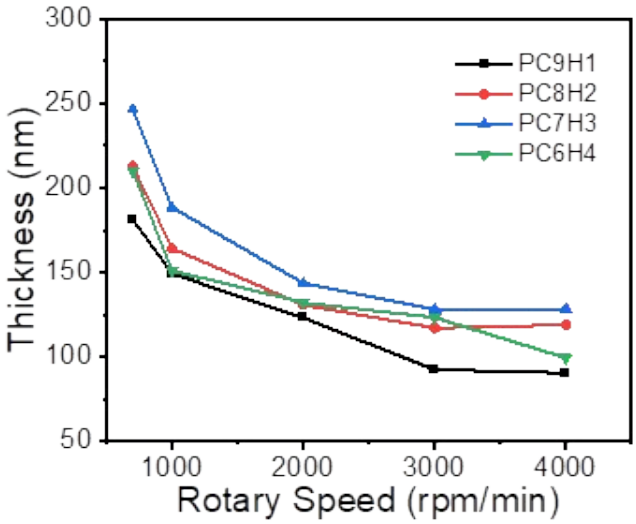

Fig. S20 The thickness curves of the P(CEA-co-HDDA) (determined by AFM) under different spin-coating speeds.

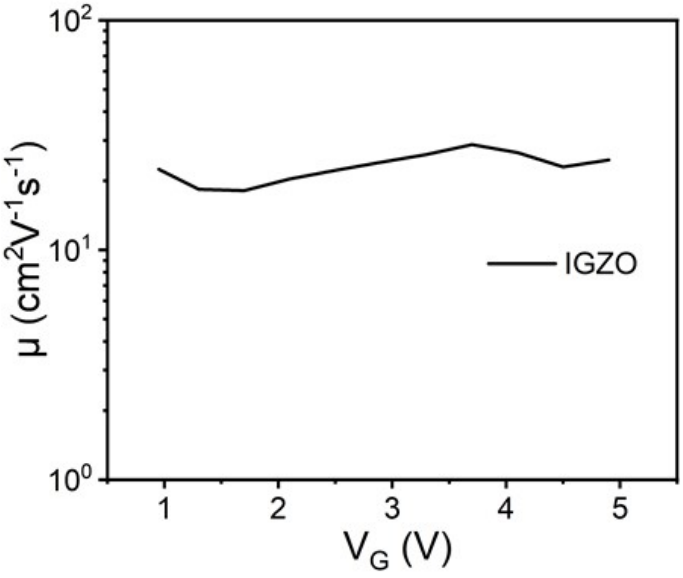

Fig. S21 Gate-voltage-dependence of the field-effect mobility in IGZO-based TFT device. The mobility is nearly constant in the saturation region, showing gate-voltage-

independent field-effect mobility.

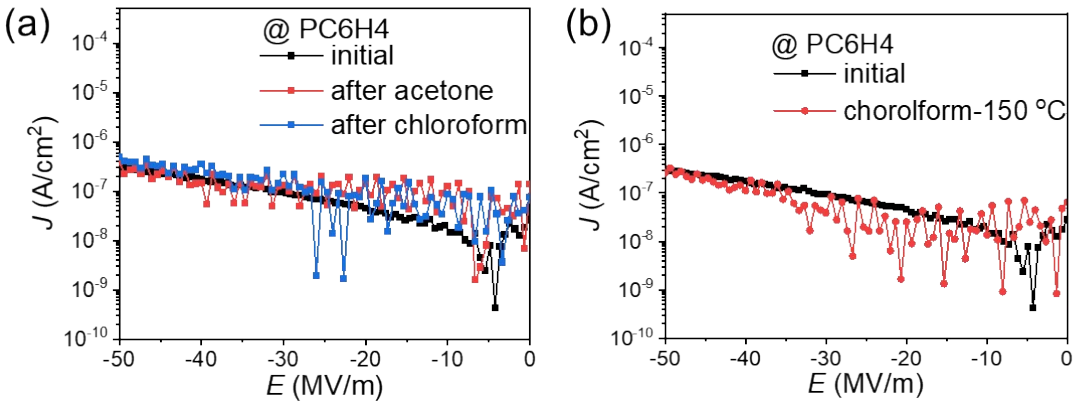

Fig. S22 The leakage current density of the PC6H4 polymer under different electric strengths under the (a) solution immersion and (b) high temperature annealing. The results show the excellent electrical stability of PC6H4 polymer to the organic-solvents and high-temperature conditions.

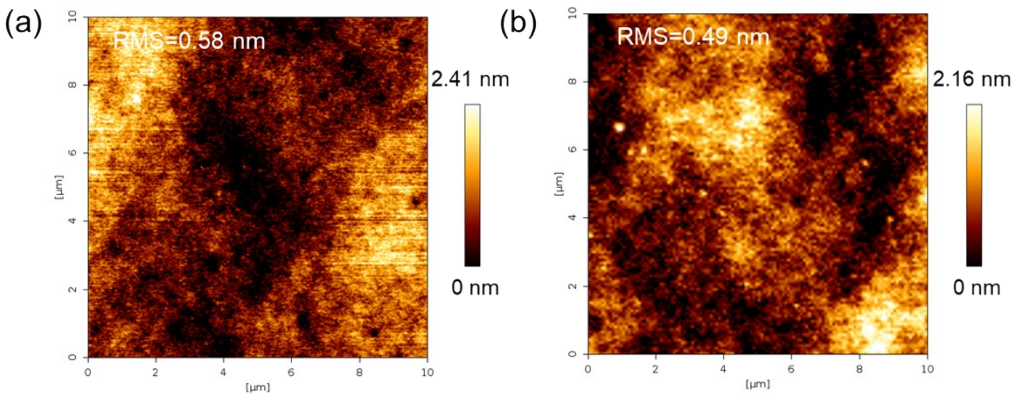

Fig. S23 Surface morphology of the PC6H4 dielectric film (a) before and (b) after chloroform treatment by AFM scanning. The results show that the RMS of the PC6H4 film is slightly altered from 0.58 nm to 0.49 nm, revealing excellent solvent-resistance property of the PC6H4 film.

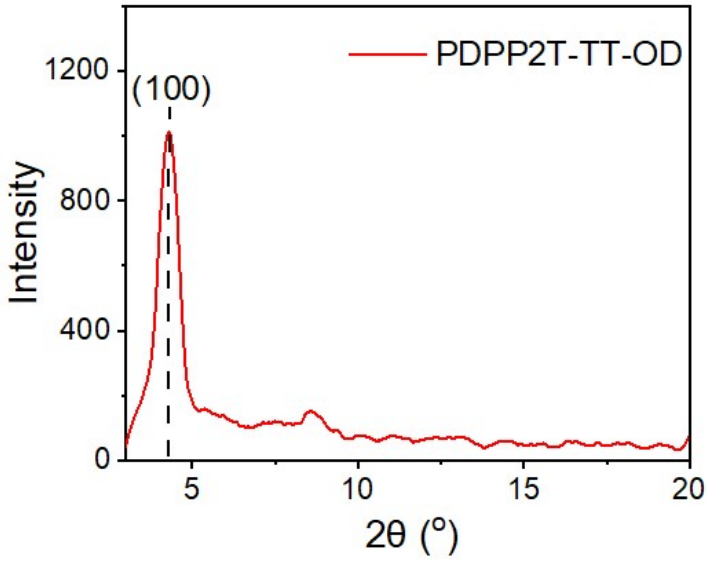

Fig. S24 XRD diagram of PDPP2T-TT-OD film. The characteristic peak at the scanning angle of 4.3° shows the crystallization of the polymeric semiconductor, which displays a high-range order and is beneficial to the high-performance OTFTs.

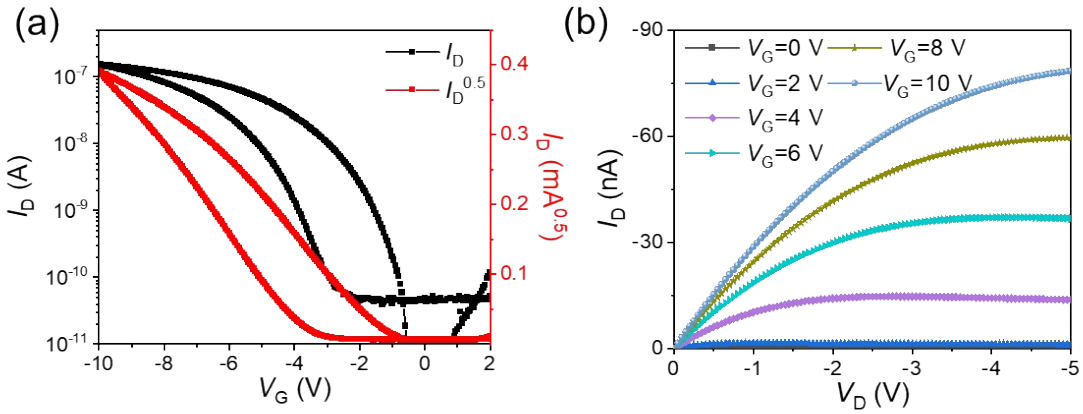

Fig. S25 Transfer and output characteristics of PDPP2T-TT-OD based TFTs on SiO_2/Si substrate. The TFTs devices exhibited a large hysteresis, which is probably induced by the interfacial trapping sites formed by the chemical functional groups on the SiO_2 surface after plasma treatment.

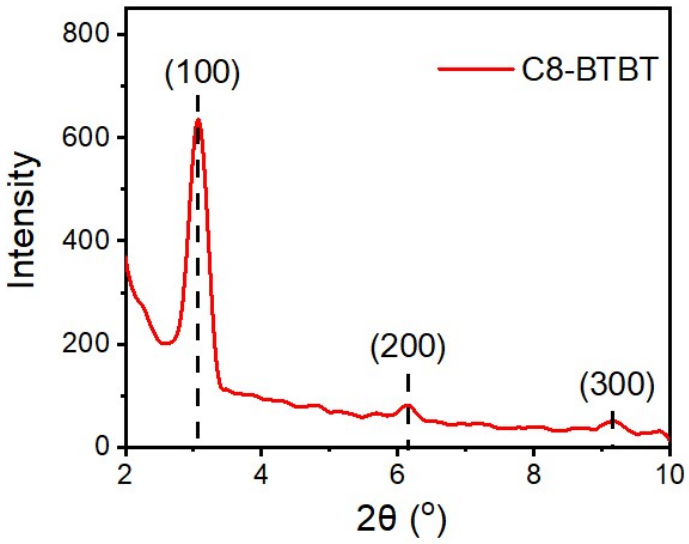

Fig. S26 The crystallization characterization of C8-BTBT by XRD. The out-of-plane d-spacing calculated to be 3.0 nm, proximately equal to the long-axis length of C8-BTBT molecules.

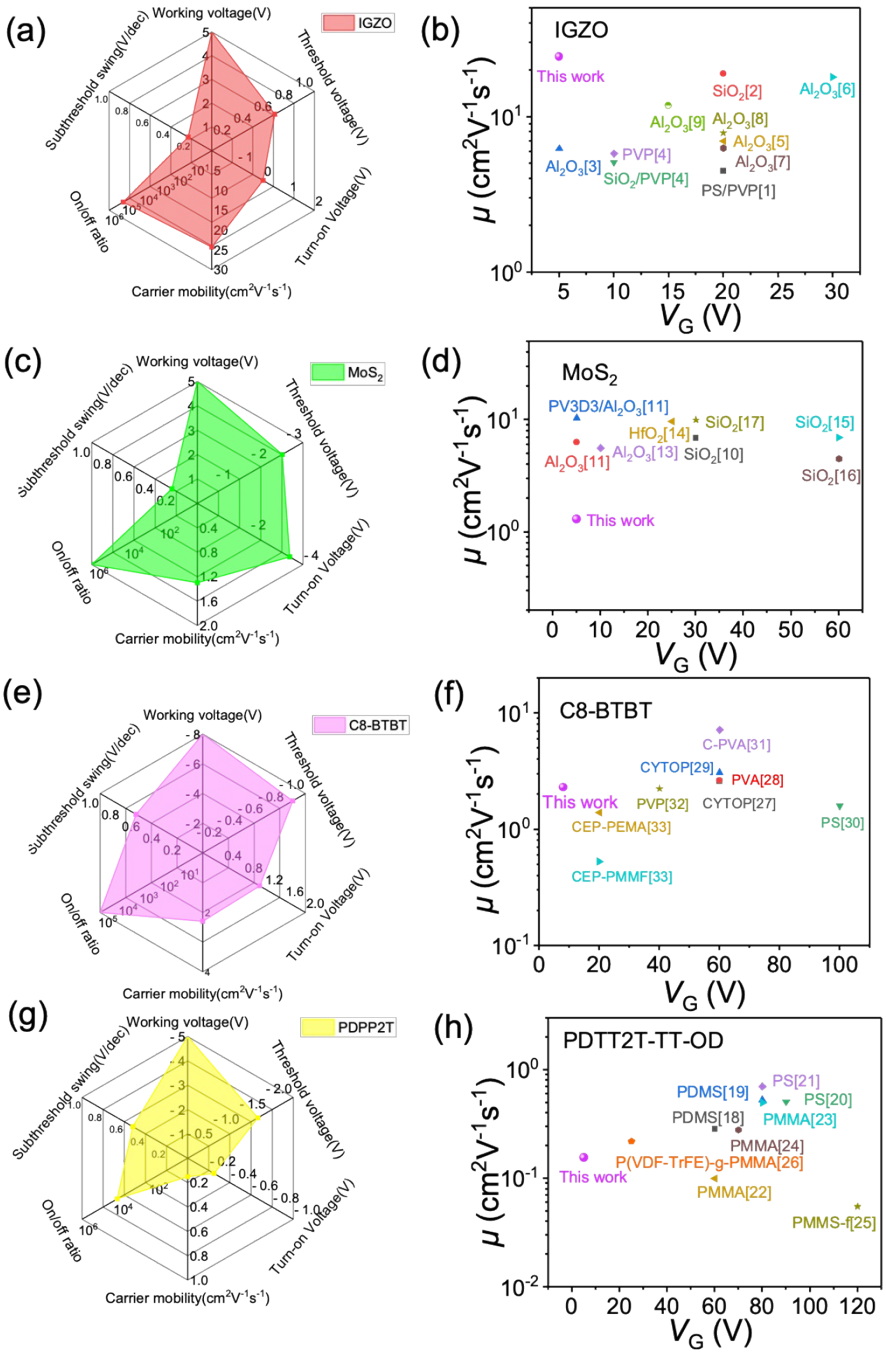

Fig. S27 Radar map and comparation on the electrical performance of the inorganic (IGZO and MoS_2) and organic (PDTT2T-TT-OD and C8-BTBT) TFTs. (a, b) IGZO-based TFTs; (c, d) MoS_2-based TFTs; (e-f) C8-BTBT-based TFTs; (g-h) PDTT2T-TT-OD-based TFTs.

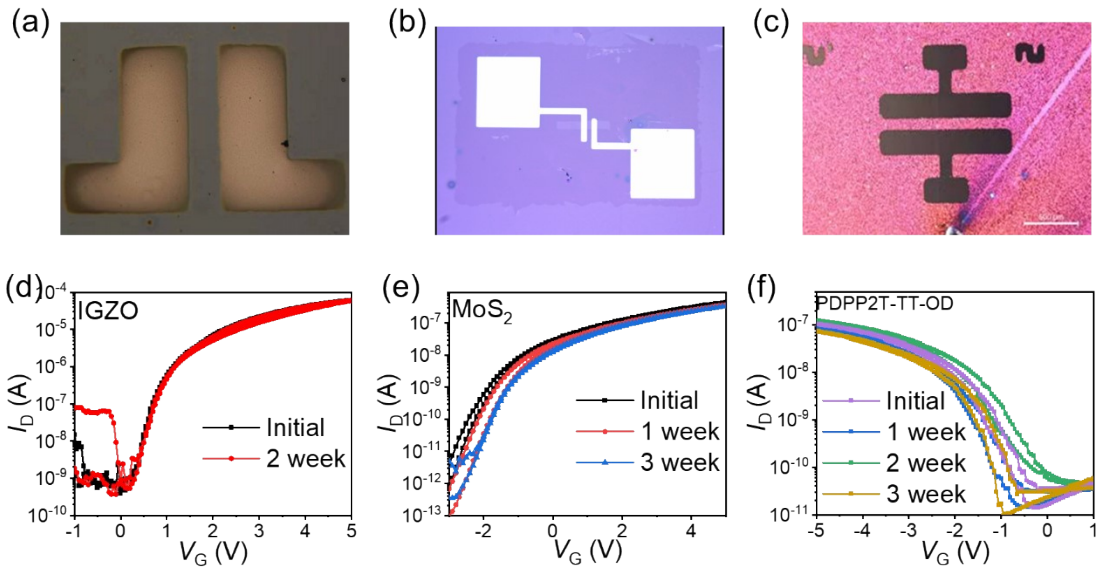

Fig. S28 The optical photographs of TFTs with different semiconductors and the transfer characteristics of relative TFTs devices with different aging times: (a, d) IGZO-based TFTs; (b, e) MoS_2-based TFTs; (c, f) PDPP2T-TT-OD-based TFTs.

Table S2. The device structure of the IGZO TFTs cited in the references

Reference number	TFT configuration
1	Bottom gate, bottom contact
2	Bottom gate, top contact
3	Bottom gate, top contact
4	Bottom gate, top contact
5	Bottom gate, top contact
6	Bottom gate, top contact
7	Bottom gate, top contact
8	Bottom gate, top contact
9	Bottom gate, top contact

Table S3. The device structure of the MoS_2 TFTs cited in the references

Reference number	TFT configuration
10	Bottom gate, bottom contact
11	Bottom gate, top contact
12	Bottom gate, top contact
13	Bottom gate, top contact
14	Bottom gate, top contact
15	Bottom gate, top contact
16	Bottom gate, top contact
17	Bottom gate, top contact

Table S4. The device structure of the PDTT2T-TT-OD TFTs cited in the references

Reference number	TFT configuration
18	Bottom gate, top contact
19	Bottom gate, bottom contact
20	Top gate, bottom contact
21	Top gate, bottom contact
22	Top gate, bottom contact
23	Top gate, bottom contact
24	Top gate, bottom contact
25	Top gate, bottom contact
26	Top gate, bottom contact

Table S5 The device structure of the C8-BTBT TFTs cited in the references

Reference number	TFT configuration
27	Top gate, bottom contact
28	Bottom gate, top contact
29	Top gate, bottom contact
30	Top gate, bottom contact
31	Bottom gate, top contact
32	Bottom gate, top contact
33	Bottom gate, top contact

References

1 M. Benwadih, R. Coppard, K. Bonrad, A. Klyszcz and D. Vuillaume, *ACS Appl Mater Interfaces*, **2016**, 8, 34513.

2 D. Koretomo, S. Hamada, M. Mori, Y. Magari and M. Furuta, *Applied Physics Express*, **2020**, 13, 076501.

3 L. Zhang, Q. Guo, Q. Tan, Z. Fan and J. Xiong, *IEEE Access*, **2019**, 7, 184312.

4 G. W. Hyung, J. X. Wang, Z. H. Li, J. R. Koo, S. J. Kwon, E. S. Cho and Y. K. Kim, *J Nanosci Nanotechnol*, **2013**, 13, 4052.

5 J. Chen, H. Ning, Z. Fang, R. Tao, C. Yang, Y. Zhou, R. Yao, M. Xu, L. Wang and J. Peng, *Journal of Physics D: Applied Physics*, **2018**, 51, 165103.

6 M. U. Cho, Y.-J. Cha, M. Byeon, Y. J. Yoon and J. S. Kwak, *Journal of the Korean Physical Society*, **2020**, 76, 715.

7 X. Ding, H. Zhang, J. Zhang, J. Li, W. Shi, X. Jiang and Z. Zhang, *Materials Science in Semiconductor Processing*, **2015**, 29, 69.

8 H. Ning, X. Zeng, H. Zhang, X. Zhang, R. Yao, X. Liu, D. Luo, Z. Xu, Q. Ye and J. Peng, *Membranes (Basel)*, **2021**, 12, 29.

9 J. Y. Bak, Y. Kang, S. Yang, H. J. Ryu, C. S. Hwang, S. Han and S. M. Yoon, *Sci Rep*, **2015**, 5, 7884.

10 P. K. Mohapatra, K. Ranganathan and A. Ismach, *Advanced Materials Interfaces*, **2020**, 7, 2001549.

11 H. Park, D. S. Oh, W. Hong, J. Kang, G. B. Lee, G. H. Shin, Y. K. Choi, S. G. Im and S. Y. Choi, *Advanced Materials Interfaces*, **2021**, 8, 2100599.

12 H. Park, J. Mun, D. Joung, J. J. Wie, S.-H. Jeong and S.-W. Kang, *Chemical Engineering Journal*, **2020**, 382, 122944.

13 W. Hong, D. S. Oh and S.-Y. Choi, *Journal of Information Display*, **2020**, 22, 13.

14 M. Zhao, L. Zhang, M. Liu, Y. Dong, C. Zou, Y. Hu, K. Yang, Y. Yang, H. Zeng and S. Huang, *Journal of Materials Science*, **2017**, 53, 4262.

15 T.-K. Park and H.-N. Lee, *Molecular Crystals and Liquid Crystals*, **2018**, 662, 2.

16 S. Zhang, H. Xu, F. Liao, Y. Sun, K. Ba, Z. Sun, Z. J. Qiu, Z. Xu, H. Zhu, L. Chen, Q. Sun, P. Zhou, W. Bao and D. W. Zhang, *Nanotechnology*, **2019**, 30, 174002.

17 J. H. Kim, T. H. Kim, H. Lee, Y. R. Park, W. Choi and C. J. Lee, *AIP Advances*, **2016**, 6, 065106.

18 R. Song, S. Yao, Y. Liu, H. Wang, J. Dong, Y. Zhu and B. T. O'Connor, *ACS Appl Mater Interfaces*, **2020**, 12, 50675.

19 S. W. Kim, S. Park, S. Lee, D. Kim, G. Lee, J. Son and K. Cho, *Advanced Functional Materials*, **2021**, 31, 2010870.

20 F. Huang, Y. Xu, Z. Pan, W. Li and J. Chu, *IEEE Electron Device Letters*, **2020**, 41, 1082.

21 F. Huang, M. Li, Y. Xu, A. Cui, W. Li, Y. Xu, J. Chu and Y.-Y. Noh, *IEEE Transactions on Electron Devices*, **2019**, 66, 2723.

22 X. Y. Chin, G. Pace, C. Soci and M. Caironi, *Journal of Materials Chemistry C*, **2017**, 5, 754.

23 H. Opoku, B. Nketia-Yawson, E.-S. Shin and Y.-Y. Noh, *Journal of Materials*

Chemistry C, **2018**, 6, 661.

24 N.-K. Kim, E.-S. Shin, Y.-Y. Noh and D.-Y. Kim, *Organic Electronics*, **2018**, 55, 6.

25 J. S. Kwon, H. W. Park, D. H. Kim and Y. J. Kwark, *ACS Appl Mater Interfaces*, **2017**, 9, 5366.

26 E.-Y. Shin, H. J. Cho, S. Jung, C. Yang and Y.-Y. Noh, *Advanced Functional Materials*, **2018**, 28, 1704780.

27 T. Endo, T. Nagase, T. Kobayashi, K. Takimiya, M. Ikeda and H. Naito, *Applied Physics Express*, **2010**, 3, 121601.

28 H. Ren, Q. Tang, Y. Tong and Y. Liu, *Materials (Basel)*, **2017**, 10, 918.

29 S. Sanda, R. Nakamichi, T. Nagase, T. Kobayashi, K. Takimiya, Y. Sadamitsu and H. Naito, *Organic Electronics*, **2019**, 69, 181.

30 T. Matsushima, A. S. Sandanayaka, Y. Esaki and C. Adachi, *Sci Rep*, **2015**, 5, 14547.

31 H. Ren, N. Cui, Q. Tang, Y. Tong, X. Zhao and Y. Liu, *Small*, **2018**, 14, 1801020.

32 W. Zhao, J. Jie, Q. Wei, Z. Lu, R. Jia, W. Deng, X. Zhang and X. Zhang, *Advanced Functional Materials*, **2019**, 29, 1902494.

33 Y.-S. Choe, M. H. Yi, J.-H. Kim, G.-S. Ryu, Y.-Y. Noh, Y. H. Kim and K.-S. Jang, *Organic Electronics*, **2016**, 36, 171.